11th World Congress on Computational Mechanics (WCCM XI)
5th European Conference on Computational Mechanics (ECCM V)
6th European Conference on Computational Fluid Dynamics (ECFD VI)
E. Oñate, J. Oliver and A. Huerta (Eds)

COMPUTATION OF THE EFFECTIVE LAMINATION STACK'S BEHAVIOR CONSIDERING THE CONTACT SIMULATION WITH A MULTI-SCALE HOMOGENIZATION

V. Luchscheider*, M.Maidorn† and K. Willner*

* Chair of Applied Mechanics
Egerlandstr. 5, 91058 Erlangen
e-mail: vera.luchscheider@ltm.uni-erlangen.de
e-mail: kai.willner@ltm.uni-erlangen.de

† Siemens AG, Industry Sector
Drive Technologies Division, Large Drives
Vogelweiherstr. 1-15, 90441 Nuremberg
e-mail: mischa.maidorn@siemens.com

Key words: Contact Mechanics, Homogenization, Lamination Stack.

Abstract. The influence of the lamination stack on the mechanical behavior of an electrical machine is significant, especially for lightweight designs. Information about the stack's behavior is relevant for a proper calculation of the whole motor. This behavior is dependent on the contact between the single sheets. This paper aims to show that the normal contact behavior can be simulated with the elastic model of Bush, Gibson and Thomas, a plastic term depending on deformation of the highest peaks and a viscous term. The tangential slip is described through a micro-macro model. These models can be used in a representative volume element and consequently for a multi-scale homogenization. A material model of the whole lamination stack can be identified by loading the representative volume element with different deformations.

1 INTRODUCTION

It is common to simulate the mechanical behavior of machines before they are built. For a proper simulation the mechanical behavior of all single parts and the different loading situations have to be known. In the case of electrical machines, the behavior of the lamination stack is unknown in detail, but it becomes relevant with the growing focus on lightweight construction. Therefore machine frames are reduced, for example, which increases the influence of the lamination stack on the machine's mechanical behavior. The aim is to identify a material model for the whole stack. This is dependent on the contact

behavior of the single sheets. Thus, the contact behavior in the normal and the tangential direction must be identified.

2 CONTACT FORMULATION

The identification and simulation of the contact behavior is usually divided into the normal and the tangential part. It has been shown by Willner [1] that there is almost no difference between the simulation with an elastic halfspace model with uncoupled directions and one with coupled directions. It is thus advisable to look at the normal and the tangential direction on their own.
The whole contact behavior is caused by the roughness peaks of the surfaces. They and the single real contacts of the peaks are responsible for both the progressive normal behavior and the nonlinear tangential behavior. A few simplifications and assumptions are common for identifying models. The surface roughness is replaced by asperities [2], with certain radii. Heights of the asperities are specified by a normal distribution in the case of technical surface without texture [3]. The number of asperities in contact is small in relation to the contact area and there is thus no interference between the deformation of the single contacts [4]. In addition, it is common to simplify the contact of two rough surfaces by using a contact of one rough surface with a rigid ideal flat surface. To simulate the same behavior, the characteristic parameters must be combined [5].

2.1 Normal behavior

The normal behavior of the stacks is progressive, elasto-plastic and viscous. The progression is caused by the sheet contacts - the closer the sheets, the higher the number of single contacts. As every contact has got a small stiffness, the behavior of the stack is progressive. The plastic behavior results from the fact that the loading of single very high asperities is larger than the yield strength σ_Y. And the viscosity is caused by the contact's behavior [6] and the existence of the coreplate varnish. The models to describe the behavior of these three effects are presented and combined in the following.
The description of the elastic progressive behavior is based on the above mentioned contact asperities and was developed by Bush, Gibson and Thomas [4], using the fractal behavior of technical surfaces. This means that a technical surface without texture correlates (for different scales) with itself. The autocorrelation function of the height data is representative for the roughness and can be rewritten as structure function [4, 7]. It is possible for technical surfaces to approximate the structure function through a formulation of Berry and Blackwell [8]. They deduced it from the theory of fractals and the theory to describe surfaces with sinus waves. The structure function

$$S(x_k) = 2\ \sigma_z \cdot \left[1 - \exp\left[-\left(\frac{x_k}{x_T}\right)\right]^{4-2\cdot D_p}\right] \tag{1}$$

is characterized by the fractal dimension D_p, the transition length x_T between the fractal and the stationary region and the root mean square roughness σ_z [5]. The stationary

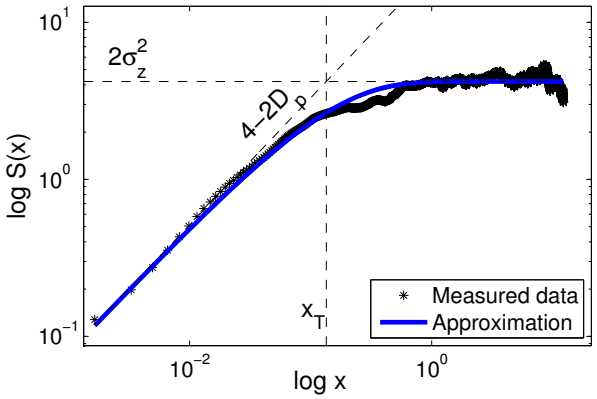

Figure 1: Example of a structure function of a coated sheet with measured data and an approximation according to equation 1

part is a consequence of the existence of a maximal roughness height (see Figure 1). For creating a contact model the fact of describing a surface with sinus waves of different wave lengths and heights is used. These waves can be identified with the autocorrelation function [7, 9] and the probability of a certain height with the joint probability function can be calculated [4, 7]. Bush, Gibson and Thomas [4] combined this function with the assumptions that the asperities are paraboloids with every possible aspect ratio and that the single contacts follow the theory of Hertz [3]. This leads to an elastic dependence of the contact pressure

$$p_{el}(g) = \frac{E^* \cdot \sigma_z^2}{2\pi \cdot x_T \cdot g} \quad \exp\left[-\frac{1}{2}\left(\frac{g}{\sigma_z}\right)^2\right] \tag{2}$$

of the gap g, which is known as the BGT model. The equivalent Hertzian modulus

$$\frac{1}{E^*} = \frac{1-\nu_1^2}{E_1} + \frac{1-\nu_2^2}{E_2} \tag{3}$$

is a combination of the elasticity moduli E_i and the Poisson constants ν_i of the materials in contact. The rms roughness $\sigma_z = \sqrt{\sigma_{z,1}^2 + \sigma_{z,2}^2}$ and the transition length $x_T = \sqrt{x_{T,1}^2 + x_{T,2}^2}$ are also combinations [5].

Plastic behavior is based on the fact that a single asperity withstands maximally a mean pressure of three times the yield strength σ_Y [10]. To identify the plastic contact behavior, the percentage of the asperities contact in ratio to the contact area is relevant. This ratio is equivalent to the cumulative normal distribution of the heights, which is also known as the Abbott-Firestone curve [11]. Consequently the plastic contact pressure

$$p_{pl}(g) = 3 \;\; \sigma_Y \;\; \frac{1}{\varsigma\sqrt{2\pi}} \int_g^\infty \exp\left[-\frac{1}{2}\left(\frac{x-\eta}{\varsigma}\right)^2\right] dx \tag{4}$$

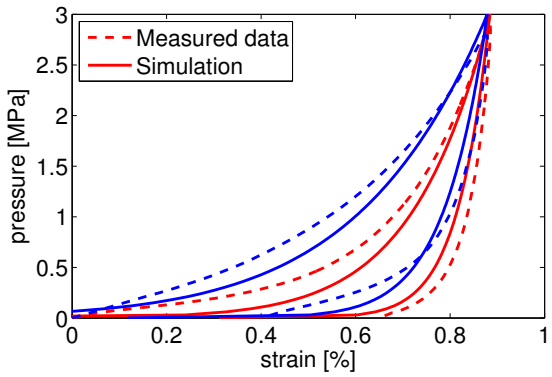

Figure 2: Measurement and simulation of the first loading and unloading of a lamination stack ($E^* = 115385\ \frac{N}{mm^2}$, $\sigma_Y = 317\ \frac{N}{mm^2}$ / red: charge A, $\sigma_z = 1.46\ \mu m$, $x_T = 0.18\ mm$, $\varsigma = 1.45\ \mu m$ and $\eta = 0.97\ \mu m$ / blue: charge B, $\sigma_z = 1.93\ \mu m$, $x_T = 0.68\ mm$, $\varsigma = 4.73\ \mu m$ and $\eta = 1.90 \mu m$)

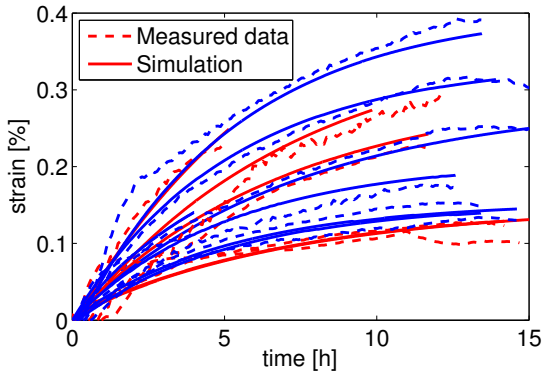

Figure 3: Measurement and simulation of a stack's creeping ($E^* = 115385\ \frac{N}{mm^2}$ / red: charge A, $\sigma_z = 1.46\ \mu m$, $x_T = 0.18\ mm$, $A = 0.00072\ \frac{mm^3}{N}$, $m = 1$ and $n = 0.137\ \frac{1}{h}$ / blue: charge B, $\sigma_z = 1.93\ \mu m$, $x_T = 0.68\ mm$, $A = 0.00079\ \frac{mm^3}{N}$, $m = 1$ and $n = 0.190\ \frac{1}{h}$)

is identified by Tsukizoe-Hisakado. ς is the standard deviation and η the expected value of the normal distribution.

Effects of creeping and relaxation are often simulated with models, which contain springs and frictional elements in different combinations [12]. The disadvantage of these models is that they are only able to simulate creeping or relaxation. As both are caused by the same reason, it is possible to calculate them with the formulation of the velocity of the creeping strain

$$\dot{\varepsilon}_{cr} = A \cdot \sigma(t)^m \cdot n \cdot \exp(-n \cdot t) \tag{5}$$

by Rust [13]. A, m and n are characteristic constants, t is the time since creeping or relaxation started and σ is the actual stress.

To simulate the actual normal behavior, the elastic and the plastic gap have to be added and the creeping strain has to be superposed. As can be seen in Figure 2 it is possible to simulate the progressive behavior of loading and unloading a lamination stack. In particular, the simulation of the elastic behavior after a first load is simulated quite well. The discrepancies between measurement and simulation during the loading are caused by effects such as the sheets waviness or the deformation of edges, which are not part of the model. The simulation of the creeping is shown in Figure 3 and fits quite well. Knowing the parameters of the creeping the relaxation is also identified.

2.2 Tangential behavior

The behavior in tangential direction is also based on the roughness and the single contacts, even though it is often simulated just by analogous models out of springs and

friction elements. These may be Jenkin or Masing models [12] and the friction is usually characterized by the Coulomb law. These models work well, but the theoretical background is minimal. For that reason a theory based on the contact behavior is used in this paper [14, 15].
Tangential behavior is dependent on the deformation and the adhesion of the single contacts. The tangential load F_T is consequently proportional to the number of contacts. Because this number is caused by the mean pressure the nominal contact area isn't relevant. This independence is the basis for the well-known contact theory of Amonton [16]. During the tangential loading, there is a small elastic deformation of the roughness peaks and a small movement in the normal direction to loosen the single connections. For this loosening the surface energy of the adhesion has to be overcome. The tangential load

$$F_T = \sigma_A \cdot A + \mu \cdot F_N \tag{6}$$

is thus dependent on the critical shear stress of the adhesion σ_A and the Amonton law $\mu \cdot F_N$ [17]. Because the contact area A of technical surfaces is very small, the first term is often neglected. For this case, the Amonton term remains, where the friction coefficient μ is affected by the materials, the duration of the contact and the velocity. The static friction coefficient is a bit larger than the dynamic one due to the small normal lift [16, 18]. Bowden and Tabor [10] found that the friction coefficient can be estimated by the shear stiffness σ_Y and the yield pressure p_Y:

$$\mu = \frac{F_T}{F_N} = \frac{\sigma_Y \cdot A}{p_Y \cdot A} = \frac{\tau}{5\tau} = 0.2 \ . \tag{7}$$

For the formulation of the elasto-plastic behavior, the model of Olofsson et al. [14, 15] is used. That model is based on the assumptions already mentioned in section 2 and is based on the behavior of a single asperity like the model of Bush, Gibson and Tabor and the one of Tsukizoe and Hisakado. The contact of single asperities is a Hertz contact for the normal and tangential direction. With using the Hertzian shear modulus [14]

$$\frac{1}{G^*} = \frac{2-\nu_1}{G_1} + \frac{2-\nu_2}{G_2} \tag{8}$$

as a combination of the shear moduli G_i and the Poisson constants ν_i of the two partners, the tangential stiffness of a single asperity is known. Slip occurs when the tangential force reaches

$$F_{T,asp} = \mu \cdot F_{N,asp} \ , \tag{9}$$

which equates to the Amonton law. As the tangential force $F_{T,asp.}$ and the normal force $F_{N,asp.}$ are known from the Hertz theory, a maximal elastic asperity deformation is computable. Integrating along the asperities' heights and frictional situation, the total tangential force

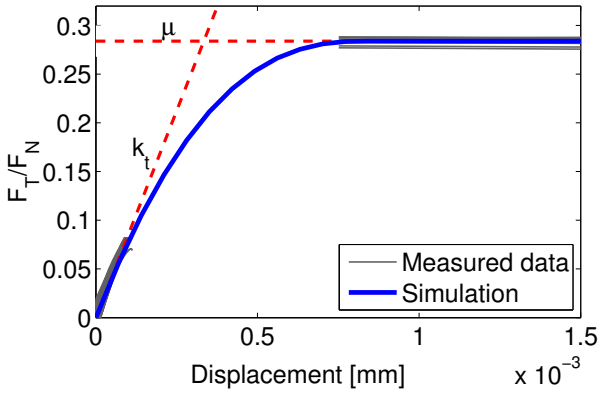

Figure 4: Measurement and simulation of the tangential sheet's slipping (as example for sheets of charge A)

$$F_T(\delta) = \frac{8}{15}\mu C A E^* \sqrt{R}\left[g^{\frac{5}{2}} - \left(g - \frac{4G^*\delta}{\mu E^*}\right)^{\frac{5}{2}}\right] \tag{10}$$

is described as a function of the tangential displacement δ. C is the number of contact asperities per unit area and R the radius of the asperities.
The microscopic contact stiffness k_t and the friction coefficient μ can be detected quite well in measurements. Tangential stiffness k_t is the stiffness of all contacts, without any gliding and therefore without an hysteretic effect. For that it is equivalent to the gradient at the start of the Olofsson model

$$k_t = \frac{8}{3} C G^* g^{\frac{3}{2}} \sqrt{R} \ . \tag{11}$$

The friction coefficient follows the maximal tangential force as shown in Amoton's law. Tangential movement in the micro-slip zone is not easily detectable in the case of single sheets. Two of the main problems are the tangential fixation of the sheets and the effects of the sheet's edges slipping over each other. In Figure 4 measured data of stiffness and friction coefficient are used to identify the micro slip behavior with the Olofsson model. The friction coefficient of 0.28 is a bit larger than expected, based on the theory of Bowden and Tabor (equation 7).

3 MULTISCALE FORMULATION

For the simulation of a whole lamination stack, a modeling of the single contacts is too expensive in time and working memory. Because of that, a multiscale homogenization is used to evolve a material model of the whole stack (Figure 5). That homogenization

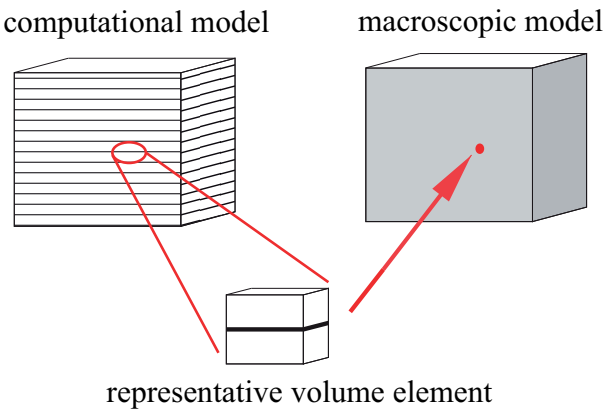

Figure 5: Principle of homogenization of a lamination stack

is based on representative volume elements (RVE) used at every integration point [19]. They contain every mechanical behavior of relevance for the stack. That is, in the case of the lamination stack, the sheet's steel and the nonlinear normal and tangential contact behavior. Another issue is that the RVEs have to fit together without any jumps in stress or strain. To achieve this, a correct volume must be chosen and periodic boundary conditions applied [19, 20]. In the stack's case, the volume has the height of a single sheet and a plane contact area in between. The periodic boundary conditions must ensure that the fitting of the RVEs is possible during the loading with a deformation gradient. In the 3-D case, there are four nodes at the RVEs' corners to which the deformation gradient is applied. All other surface nodes are connected to these four nodes in a way that all edges and surfaces are deformed like the ones on the opposite side. It is thus possible for every deformation gradient to fit the RVEs together.
To calculate with homogenization, every integration point of the macroscopic model is calculated with the RVE. Therefore, the Taylor hypothesis [19] postulates the mean microscopic deformation gradient

$$\overline{\underline{\underline{F}}_m} = \frac{1}{V_0} \int_{V_0} \underline{\underline{F}}_m \; dV_0 = \underline{\underline{F}}_M \tag{12}$$

to be the macroscopic deformation gradient $\underline{\underline{F}}_M$ at the integration point. That can be done because the periodic boundary conditions lead to zero for the gradient's term of fluctuation $\nabla\overrightarrow{\omega}$ of integrating it along the surface Γ_0 of the RVE [20]. With the periodic deformation, the stress field and the surface forces $\underline{p}$ at the RVE are calculated. As the nonlinear contact is also part of the calculation, the resulting stresses are contact-dependent. To identify the stress situation at the integration point, a resizing and homogenization to the macroscopic scale is necessary. The mean first Piola-Kirchhoff stress tensor of the microscopic scale

$$\overline{\underline{\underline{P}}_m} = \frac{1}{V_0} \int_{\Gamma_0} \underline{p} \otimes \underline{x}_m \; dA \tag{13}$$

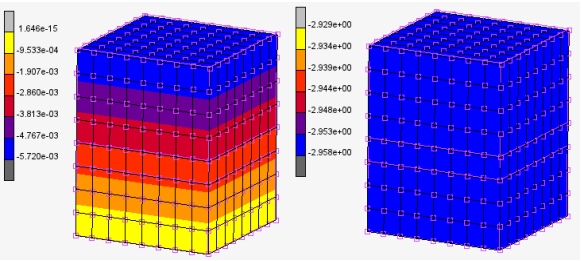

a) Normal displacement [mm] and stress [MPa] of the RVE

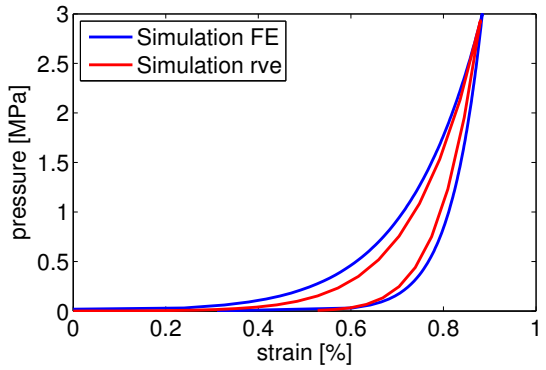

b) Loading and unloading of an FE-model (blue) and the RVE (red)

Figure 6: Normal load (example for sheets charge A)

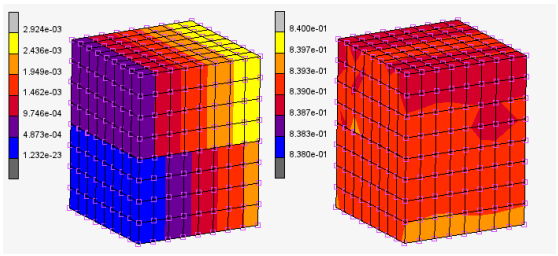

a) Tangential displacement [mm] and stress [MPa] of the RVE

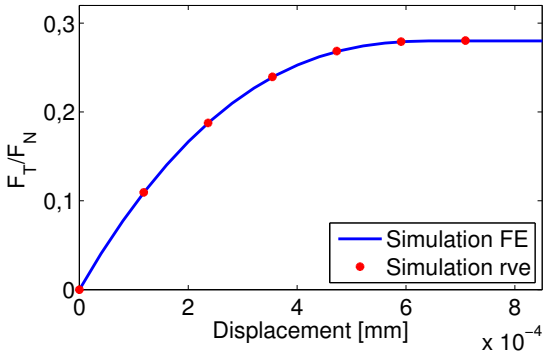

b) Tangential loading of an FE-model (blue) and the RVE (red)

Figure 7: Tangential load (example for sheets charge A)

is dependent on the surface forces $\underline{p}$ and the displacement $\underline{x}_m$. The Hill-Mandel hypothesis [20] equalizes the average power density of the RVE and the integration point

$$\underline{\underline{P}}_M : \delta\underline{\underline{F}}_M = \frac{1}{V_0}\int_{V_0} \underline{\underline{P}}_m : \delta\underline{\underline{F}}_m \; dV \quad . \tag{14}$$

Combined with the Gaussian integration rule, the dependencies of the deformation gradients (equation 12) and the mean first Piola-Kirchhoff stress tensor (equation 13), it can be seen that [19]

$$\overline{\underline{\underline{P}}_m} = \underline{\underline{P}}_M \quad . \tag{15}$$

The identification of a stack's material model is performed by applying different loading situations of pressure and shear onto the RVE. Due to the non-linearity of the contact, the created stiffness and damping matrices are also non-linear.
The RVE in use is depicted in Figure 6 a and Figure 7 a. At first it is loaded with a normal displacement (Figure 6 a) left), what causes a unique normal stress (Figure 6 a) right) and tangential displacements and stresses to keep constant volume. Afterward, a small tangential displacement (Figure 7 a) left) is superposed. The consistent shear stress, which has only small numerical variations, is depicted on the right of Figure 7 a).

Because periodic boundary conditions are used, the tangential displacement must be smaller than the width of an FE element in the RVE. Otherwise the surface of the RVE volume changes too much and new periodic boundary conditions must be introduced. The actual calculation complies with this small displacement, because the micro-slip zone is very small and it is sufficient to reach macro-slip. The congruence of the normal and tangential behavior of the RVE (Figure 6 b and Figure 7 b) with the simulations of Figure 2 and Figure 4 illustrates that all mechanically relevant characteristics are part of the RVE. With that, it is feasible to calculate the behavior of a whole stack by using multi-scale homogenization.

4 CONCLUSION

This paper presents a possible way to simulate the behavior of lamination stacks. The basis is the simulation of the sheet's contacts. They are motivated by the surface roughness and the behavior of single peaks in contact. Both the number and behavior of the single contacts are known and consequently models describing the behavior of two surfaces in contact have been developed [4, 11, 15]. For a proper use of these models and to reduce the working memory space, a multi-scale homogenization is utilized in this paper. With this homogenization, it is possible to simulate the stack's behavior for every reasonable loading situation, therefore enabling a material model for the stack to be created. The material model permits an easy and fast calculation of the mechanical behavior of the whole stack and a better calculation of the whole electric motor.

REFERENCES

[1] Willner, K. Fully Coupled Frictional Contact Using Elastic Halfspace Theory. *J. Tribol.* (2008) **130:** 3.

[2] Archard, J. F. Elastic Deformation and the Laws of Friction. *Proc. R. Soc. Lond. A* (1957) **243:** 190-205.

[3] Greenwood, J. A. and Williamson, J. B. P. Contact of Nominally Flat Surfaces. *Proc. R. Soc. Lond. A* (1966) **295**: 300-319.

[4] Bush, A. W., Gibson, R. D. and Thomas, T. R. The elastic contact of a rough surface. *Wear* (1975) **35**: 87-111.

[5] Willner, K. Influence of Surface Parameters on the Elastoplastic Contact Behavior of Fractal-Regular Surfaces. *J. Tribol.* (2008) **130**: 2.

[6] Al-Bender, F., Lampaert, V. and Swevers, J. A novel generic model at asperity level for dry friction force dynamics. *Tribol. Lett.* (2004) **16**: 81-93.

[7] Nayak, P. R. Random Process Model of Rough Surfaces. *J. of Lubrication Tech.* (1971) 398-407.

[8] Berry, M. V. and Blackwell, T. M. Diffractal Echoes. *J. Phys. A: Math. Theor.* (1981) **14**: 3101-3110.

[9] Longuet-Higgins, M. S. The Statistical Analysis of a Random, Moving Surface. *Phil. Trans. R. Soc. A.* (1957) **249**: 321-387.

[10] Bowden, F. P. and Tabor, D. *The Friction and Lubrication of Solids*. Oxford University Press (1950).

[11] Tsukizoe, T. and Hisakado, T. On the Mechanism of Contact Between Metal Surfaces - The Penetrating Depth and the Average Clearance. *J. Basic. Eng.* (1965) **87**: 3, 666-674.

[12] Kolsch, H. and Ottl, D. Simulation des mechanischen Verhaltens von Bauteilen mit statischer Hysterese. *Forschung im Ingenieurwesen* (1993) **59**: 66-71.

[13] Rust, W. *Nichtlineare Finite-Elemente-Berechungen: Kontakt, Geometrie, Material*. Vieweg+Teubner Verlag, Second Edition (2011).

[14] Olofsson, U. Cyclic micro-slip under unlubricated conditions. *Tribol. Internat.* (1995) **28**: 207-217.

[15] Sellgren, U. and Olofsson, U. Application of a constitutive model for micro-slip in finite element analysis. *Comput. Methods Appl. Mech. Engrg.* (1999) **170**: 65-77.

[16] Besson, U. Historical Scientific Models and Theories as Resources for Learning and Teaching: The Case of Friction. *Sci & Educ* (2012).

[17] Berman, A., Drummond, C. and Israelachvili, J. Amontons' law at the molecular level. *Tribol. Lett.* (1998) **4**: 95-101.

[18] Gitis, N. V. and Volpe, L. Nature of static friction time dependence. *J. Phys. D: Appl. Phys.* (1992) **25**: 605-612.

[19] Miehe, C. Computational micro-to-macro transitions for discretized micro-structures of heterogeneous materials at nite strains based on the minimization of averaged incremental energy. *Comput. Methods Appl. Mech. Engrg.* (2003) **192**: 559-591.

[20] Kouznetsova, V. G., Geers, M. G. D. and Brekelmans, W. A. M. Multi-scale second-order computational homogenization of multi-phase materials: a nested finite element solution strategy. *Comput. Methods Appl. Mech. Engrg.* (2004) **193**: 5525-5550.